Available online at www.sciencedirect.com
ScienceDirect
Ceramics International 37 (2011) 1409–1414
CERAMICS INTERNATIONAL
www.elsevier.com/locate/ceramint

Pulse aging behavior of $ZnO–Pr_6O_{11}–CoO–Cr_2O_3–Dy_2O_3$ varistor ceramics with sintering time

Choon-W. Nahm

Semiconductor Ceramics Lab., Department of Electrical Engineering, Dongeui University, Busan 614-714, Republic of Korea

Received 14 September 2010; received in revised form 19 November 2010; accepted 5 January 2011
Available online 3 February 2011

Abstract

The aging behavior against a pulse-current in the $ZnO–Pr_6O_{11}–CoO–Cr_2O_3–Dy_2O_3$ varistor ceramics was investigated in accordance with sintering time. The varistors sintered for 1 h exhibited the best clamp characteristics; the clamping voltage ratio was in the range of 1.69–1.92 for the lower pulse-current region (5–50 A) and in the range of 2.0–2.98 for the higher pulse-current region (400–1800 A). The best electrical stability against a pulse-current was obtained by the varistor ceramics sintered for 3 h, with $\%\Delta E_{1\,mA/cm^2} = -7.2\%$, $\%\Delta\alpha = -21.9\%$, and $\%\Delta J_L = 13.0\%$ after applying the multi-pulse current of 1800 A.

Keywords: A. Sintering; E. Varistors; Electrical measurement; Pulse-current; Aging

1. Introduction

The sintered pellet of pure zinc oxide is a polycrystalline ceramics containing many grains and exhibits ohmic characteristics, which the current increases linearly in accordance with increasing voltage. On the contrary, the zinc oxide ceramics added with specific impurities exhibits varistor effect, where the voltage–current (*V–I*) relation is nonlinear. The zinc oxide varistors are semiconducting solid-state electronic devices formed by sintering zinc oxide with minor additives, such as bismuth, praseodymium, vanadium, and barium. They are voltage-dependent nonlinear resistors, whose resistance decreases drastically when voltage is increased up to threshold voltage, called varistor voltage. In other words, at low voltage, the varistor acts as a conventional high value resistor obeying ohms law. They play a similar role to back-to-back Zener diode. However, they possess an excellent surge absorption capability because the zinc oxide varistors are multi-junction devices, which consisted of the microstructure of SIS (semiconducting ZnO grain–insulating intergranular layer–semiconducting ZnO grain), unlike the Zener diode of single junction [1]. The zinc oxide varistors have been used extensively in the field of circuit overvoltage protection, with application ranging from a few volts in electronic circuits to millions of volts in electric power systems [2,3].

Most commercial varistors are the Zn–Bi-based varistors. However, they have a few drawbacks due to the high volatility and reactivity of Bi_2O_3 during liquid sintering [4]. The former changes varistor characteristics with a variation of inter-composition ratio of additives. The latter destroys the multi-layer structure of chip varistors, and it generates an insulating spinel phase. This phase acts as a growth moderator for ZnO grains, but plays no role in the nonlinear characteristics [5]. Furthermore, it also deteriorates the surge absorption capabilities due to a decrease of effective grain boundary area. To overcome these problems, Zn–Pr-based varistors have been actively studied [6–8]. Zn–Pr-based varistors have been studied to further enhance varistor properties and the stability against various stresses, compared to Zn–Bi-based varistors. Most investigations on Zn–Pr-based varistors have been reported on the microstructure and electrical properties in terms of additives and sintering processing [6–16]. In particular, Nahm et al. reported the effect of rare earth oxides and lanthanum oxide on electrical properties and its stability against DC accelerated degradation stress [9–17].

Important factors that should be considered in the application of varistor are the nonlinearity, its stability, and surge absorption capability. The electronic equipments and the electrical power systems, which should be protected from

E-mail address: cwnahm@deu.ac.kr.

0272-8842/$36.00
doi:10.1016/j.ceramint.2011.01.011

various surges significantly demand a high stability of varistors in order to enhance reliability. Therefore, the electrical stability against a pulse-current is technologically very important in zinc oxide varistors. However, studies on the effect of the sintering process on the surge clamping characteristics and electrical behavior of the varistors against a surge with high energy have been slightly reported [18–23]. In this work, the effects of the sintering time on pulse aging behavior of the ZnO–Pr_6O_{11}–CoO–Cr_2O_3–Dy_2O_3 varistor ceramics were addressed and some significant results were obtained.

2. Experimental procedure

2.1. Sample preparation

Reagent-grade raw materials were used in proportions of 97.5 mol% ZnO, 0.5 mol% Pr_6O_{11}, 1.0 mol% CoO, 0.5 mol% Cr_2O_3, and 0.5 mol% Dy_2O_3. Raw materials were mixed by ball milling with zirconia balls and acetone in a polypropylene bottle for 24 h. The mixture was dried at 120 °C for 12 h and calcined in air at 750 °C for 2 h. The calcined mixture was pulverized using an agate mortar/pestle and after 2 wt% polyvinyl alcohol (PVA) binder addition, granulated by sieving through a 100-mesh screen to produce the starting powder. The powder was uniaxially pressed into discs of 10 mm in diameter and 2 mm in thickness at a pressure of 80 MPa. The discs were sintered for three different times (1 h, 2 h, and 3 h) at 1350 °C and furnace-cooled to room temperature. The heating and cooling rates were 4 °C/min. The sintered samples were lapped and polished. The final samples were about 8 mm in diameter and 1.0 mm in thickness. Silver paste was coated on both faces of the samples and the electrodes were formed by heating it at 600 °C for 10 min. The electrodes were 5 mm in diameter.

2.2. Microstructure characterization

For microstructure characterization, both surfaces of the samples were lapped and ground with SiC paper and polished with 0.3 μm-Al powder to a mirror-like surface. The polished samples were thermally etched at 1100 °C for 30 min. The surface microstructure was examined by a scanning electron microscope (SEM, Hitachi S2400, Chiyoda-Ku, Tokyo, Japan). The average grain size (d) was determined by the lineal intercept method, given by $d = 1.56L/(MN)$, where L is the random line length on the micrograph, M is the magnification of the micrograph, and N is the number of the grain boundaries intercepted by the lines [24]. The sintered density (ρ) was measured using a density determination kit (238490) attached to a balance (AG 245, Mettler Toledo International Inc., Greifensee, Switzerland).

2.3. Electrical measurement

The electric field–current density (E–J) characteristics were measured using a high voltage source-measure unit (Keithley 237, Keithley Instruments Inc., Cleveland, OH, USA). The breakdown field ($E_{1\,mA/cm^2}$) was measured at 1.0 mA/cm^2 and the leakage current density (J_L) was measured at $0.8E_{1\,mA/cm^2}$. In addition, the nonlinear coefficient (α) is defined by the empirical law, $J = C{\cdot}E^{\alpha}$, where J is the current density, E is the applied electric field, and C is a constant. α was determined in the current density range of 1.0 mA/cm^2 to 10 mA/cm^2, where $\alpha = 1/(\log E_2 - \log E_1)$, and E_1 and E_2 are the electric fields corresponding to 1.0 mA/cm^2 and 10 mA/cm^2, respectively.

2.4. Clamping voltage measurement

The clamping voltage (V_c) was measured at a single pulse-current (I_p) of 5, 10, 25, and 50 A with 8 × 20 μs waveform using a surge generator (Tae-yang Eng., Busan, Korea) and an oscilloscope (TeK 3020B, Tektronix Inc., Beaverton, OR, USA). The pulse-current had a width of 20 μs and a rise time of 8 μs. The clamp voltage ratio ($K = V_c/V_{1\,mA}$) is defined by the ratio of clamping voltage to breakdown voltage. The breakdown voltage ($V_{1\,mA}$) was measured at a current of 1.0 mA DC.

2.5. Pulse-current aging test

The pulse-current aging test was performed at a multi-pulse current of 400, 900, 1200, 1500, and 1800 A (continuously 3 times for each pulse current) using a surge generator. The pulse-current had a width of 20 μs and a rise time of 8 μs. The time interval between multi-pulse current of 3 times was 2 min. The time interval between each pulse-current cycle was 10 min. After applying the respective pulse-current, the V–I characteristics were measured at room temperature.

3. Results and discussion

Fig. 1 shows SEM micrographs of the samples for different sintering times. There is no remarkable difference in the phases, which consisted of ZnO grains and intergranular layers in accordance with sintering time. XRD analysis (not shown) reveals the presence of minor Pr-rich and Dy-rich intergranular secondary phase, in addition to a major phase of hexagonal ZnO [14]. The average grain size (d) increased in the order of 11.5, 15.2, and 19.0 μm in accordance with increasing sintering time. The sintered density (ρ) for the samples increased in the order of 5.43, 5.54, and 5.64 g/cm^3 (theoretical density 5.78 g/cm^3 for ZnO). Therefore, the sintering time in the study for this composition significantly modified the densification process [14].

Fig. 2 shows the E–J characteristics of the samples for different sintering times. The conduction characteristics of varistors are divided into a linear region with a much higher impedance before the breakdown field and a nonlinear region with a much lower impedance after the breakdown field. The E–J characteristic parameters calculated from Fig. 2 are summarized in Table 1. The breakdown field ($E_{1\,mA/cm^2}$) decreased significantly in a wide range from 2168 to 1421 V/cm in accordance with increasing sintering time. This is attributed to the decrease in the number of grain boundaries caused by the increase in the ZnO grain size. On the other hand, the nonlinear coefficient (α) decreased from 66 to 43 in

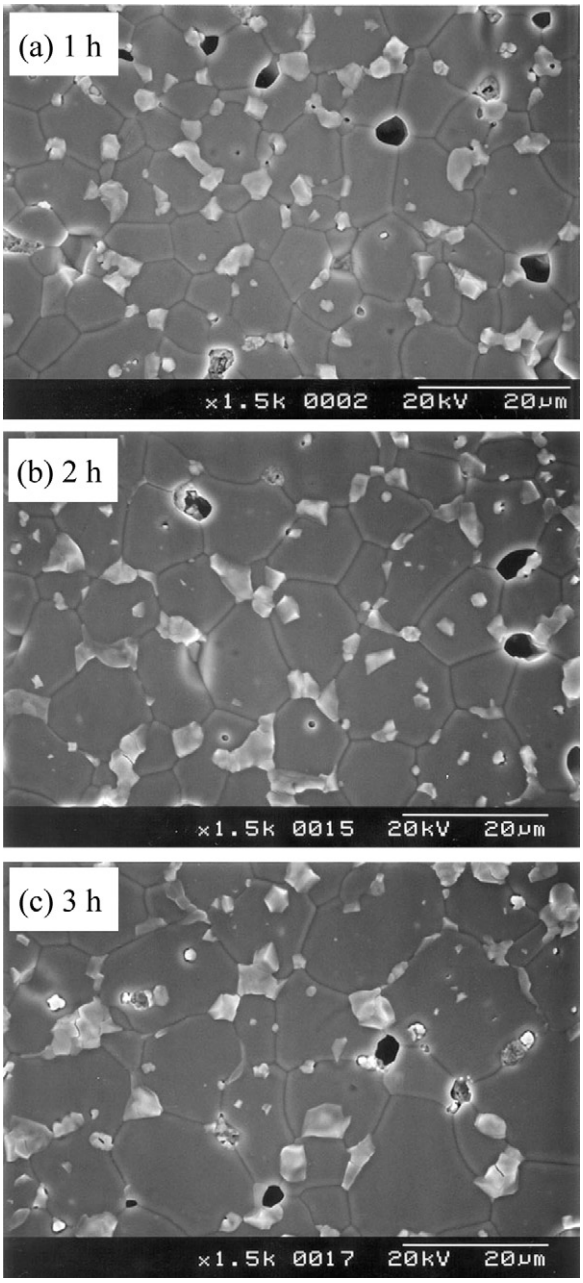

Fig. 1. SEM micrographs of the samples for different sintering times.

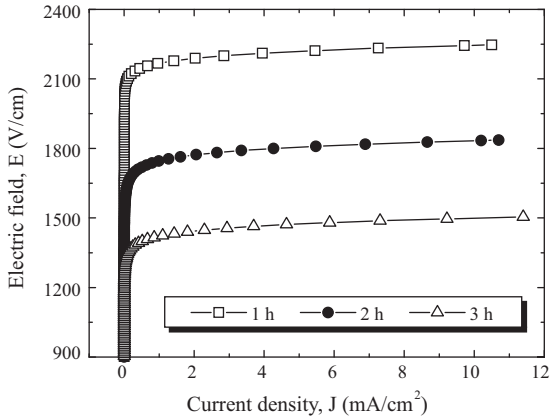

Fig. 2. *E–J* characteristic curves of the samples for different sintering times.

accordance with increasing sintering time. The decrease in α value is attributed to the lowering of the Schottky barrier because of the variation of the electronic state at the grain boundaries [14]. On the whole, the α value exhibited to be high in the range of the specified sintering times.

The clamping voltage (V_c) and clamp voltage ratio (K) corresponding to a lower pulse-current (5–50 A) for different sintering times are summarized in Table 1. The V_c is defined by the drop voltage between electrodes of the sample when the specified pulse-current flows through the sample. The higher pulse-current leads to the higher V_c because the resistance in the nonlinear region shows still as a low value [19–21]. It can be seen that the higher breakdown voltage leads to the higher clamping voltage. The low K value means that the varistor clamps a pulse-current to the operating voltage. The K value with sintering times increased up to 2 h for the specified pulse-current, whereas thereafter it decreased. The samples sintered for 1 h exhibited a minimum K value, which is 1.93 at a pulse-current of 50 A. All the samples exhibited good clamp characteristics, as recording clamping ratio less than 2 in K.

Fig. 3 shows the clamping voltage (V_c) characteristics corresponding to a multi-pulse current of 900 A and 1800 A for different sintering times. The clamping voltage (V_c) and clamp voltage ratio (K) corresponding to a higher pulse-current (400–1800 A) for different sintering times are summarized in Table 2. The K value for all the samples greatly increased in the higher pulse-current region (400–1800 A). The K value varied in the same way as the low pulse-current region (5–50 A) in accordance with increasing sintering time. Based on the α and K value in Tables 1 and 2, it can be seen that a higher α value does not necessarily lead to a low K value. In order to obtain a low K value, the α measured in the range of 1.0 mA/cm^2 and 10 mA/cm^2 have to be maintained up to high current region. Based on the data shown in Tables 1 and 2, it can be seen that the samples sintered for 1 h show the best clamping characteristics for a pulse-current.

Table 1
E–J characteristic parameters, clamping voltage (V_c), and clamp voltage ratio (K) of the samples for different sintering times.

Sintering time	$E_{1\,mA/cm^2}$ (V/cm)	α	$V_{1\,mA}$ (V/mm)	V_c (V)				$K = V_c/V_{1\,mA}$			
				I_p = 5 A	10 A	25 A	50 A	I_p = 5 A	10 A	25 A	50 A
1 h	2168	66.0	222.2	376	384	404	428	1.69	1.73	1.82	1.93
2 h	1747	47.9	180.9	296	324	348	368	1.63	1.79	1.92	2.0
3 h	1421	43.0	147.5	248	260	280	292	1.68	1.76	1.90	1.98

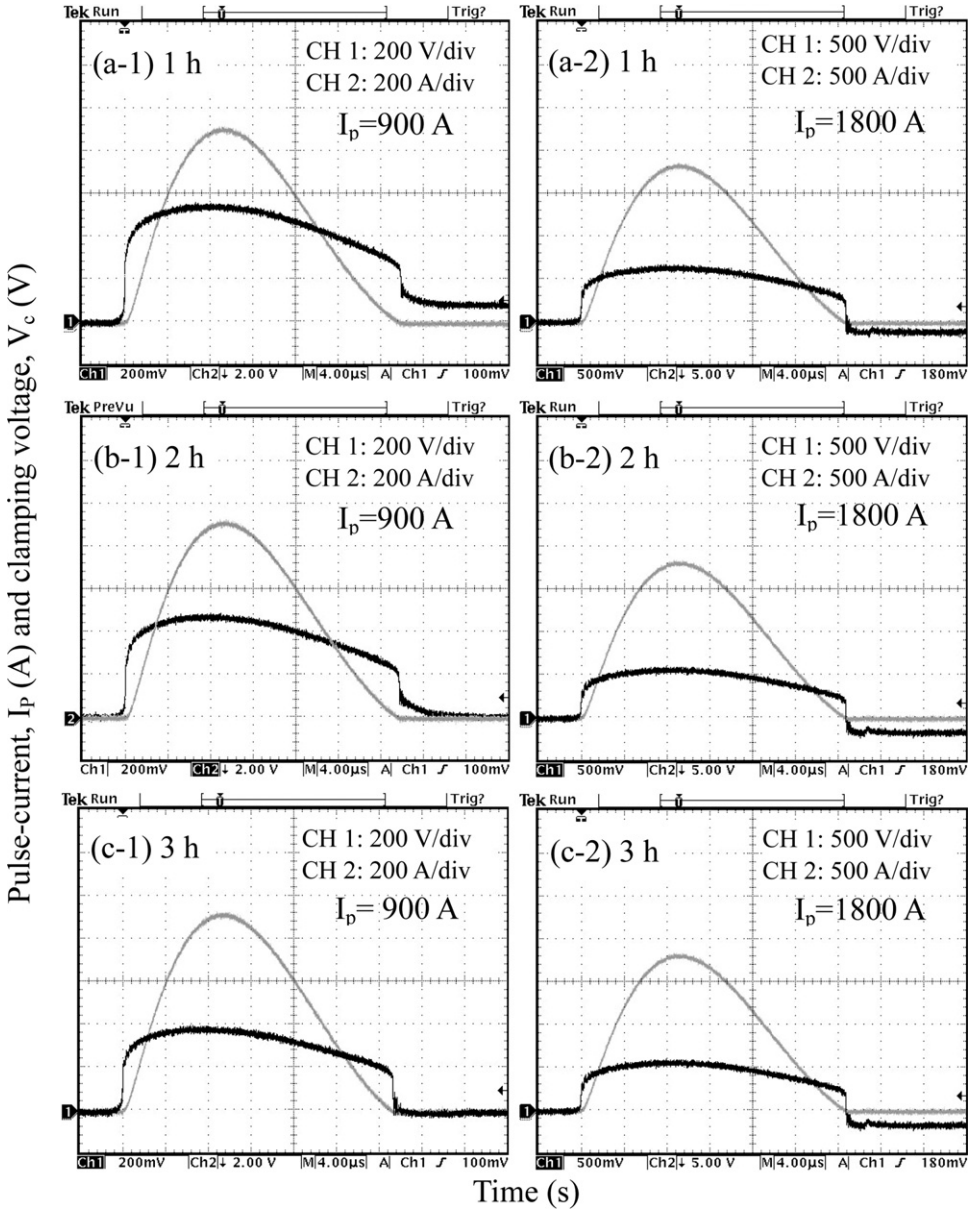

Fig. 3. Clamping voltage waveform of the samples for different sintering times for a multi-pulse current of 900 A and 1800 A.

Fig. 4 compares the variation of *E–J* characteristics after applying the higher pulse-current of 400–1800 A with the initial *E–J* characteristics for different sintering times. It can be seen that the *E–J* characteristic curve shifted toward a low field region (downward in Fig. 4) in the breakdown region after applying the pulse-current. The samples sintered for 3 h exhibited the smallest variation of *E–J* characteristics in the nonlinear region. On the contrary, the samples sintered for 2 h exhibited the largest variation in the nonlinear region. When a multi-pulse current beyond 1500 A was applied to each sample, the *E–J* characteristics greatly varied compared to the pulse-current of 900 A. On the whole, the samples sintered for 3 h exhibited a much higher stable *E–J* characteristics, compared to the other samples.

Fig. 5 compares the variation of breakdown field ($\%\Delta E_{1\,mA/cm^2}$) for different sintering times after applying the pulse-current with the initial state. By applying the multi-pulse current up to 1200 A, the samples sintered for 1 h exhibited the best *E–J* characteristics. However, the $\%\Delta E_{1\,mA/cm^2}$ after applying the multi-pulse current of 1800 A was −13.6% for the samples sintered for 1 h, −25% for the samples sintered for 2 h, and −7.2% for the samples sintered for 3 h. Therefore, the samples sintered for 3 h showed the most stable $E_{1\,mA/cm^2}$ characteristics against a multi-pulse current. On the contrary, the samples sintered for 2 h exhibited the most unstable breakdown field against a multi-pulse current.

Fig. 6 compares the variation of nonlinear coefficient ($\%\Delta\alpha$) for different sintering times after applying the multi-pulse current with the initial state. The samples sintered for 1 h and 3 h exhibited good α-characteristics of less than 10% after applying the multi-pulse current of 1200 A. When a multi-pulse current is 1500 A, only samples sintered for 3 h were less than

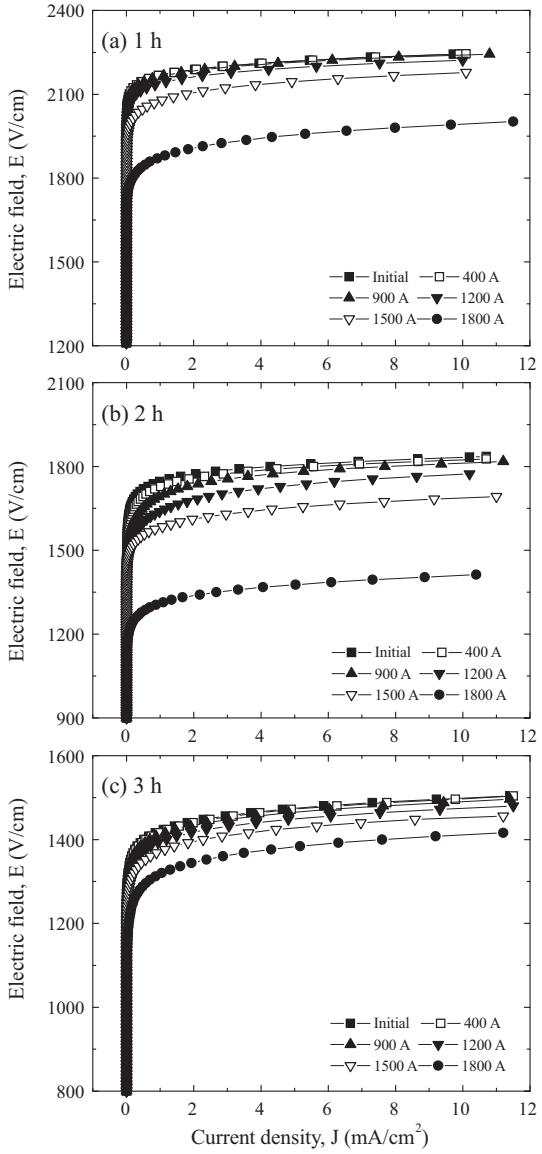

Fig. 4. *E–J* characteristic curves of the samples for different sintering times before and after applying the multi-pulse current.

Table 2
Variations of varistor voltage ($V_{1\ mA}$), clamping voltage (V_c), and clamp voltage ratio (K) of the samples for different sintering times after applying the multi-pulse stress.

Sintering time	I_p (A)	$V_{1\ mA}$ (V/mm)	V_c (V)	K
1 h	400	222.2	444	2.00
	900	221.9	544	2.45
	1200	221.5	584	2.64
	1500	219.6	605	2.76
	1800	214.6	640	2.98
2 h	400	180.9	404	2.23
	900	179.6	472	2.63
	1200	178.0	516	2.90
	1500	173.4	545	3.14
	1800	165.5	560	3.38
3 h	400	147.5	316	2.14
	900	147.3	380	2.58
	1200	146.6	414	2.82
	1500	145.0	435	3.00
	1800	142.8	460	3.22

10%. The $\%\Delta\alpha$ after applying the multi-pulse current of 1800 A was −43% for the samples sintered for 1 h, −35.1% for the samples sintered for 2 h, and −21.9% for the samples sintered for 3 h. All the samples accompanied a large variation of α at high current strength of 1800 A. As a result, it can be seen that the samples sintered for 3 h exhibited higher stability against a pulse-current than other samples, like the breakdown field behavior after applying the multi-pulse current.

Fig. 7 compares the variation of leakage current density ($\%\Delta J_L$) for different sintering times after applying the pulse-current with the initial state. The $\%\Delta J_L$ after applying the multi-pulse current of 1800 A was −18.6%, −60%, and 13.0% in accordance with increasing sintering time. The samples sintered for 3 h exhibited the best leakage current characteristics against applying the multi-pulse current, like the nonlinear coefficient and breakdown field behavior after applying the multi-pulse current. As a result, it can be seen that the sintering time has a significant effect on the stability against a pulse-current. Conclusively, It was found that these

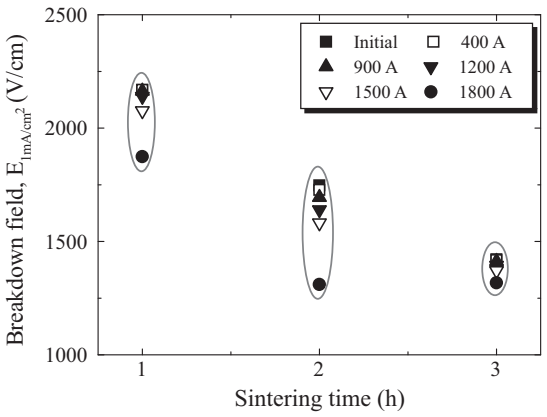

Fig. 5. Variation of breakdown field of the samples for different sintering times after applying the multi-pulse current.

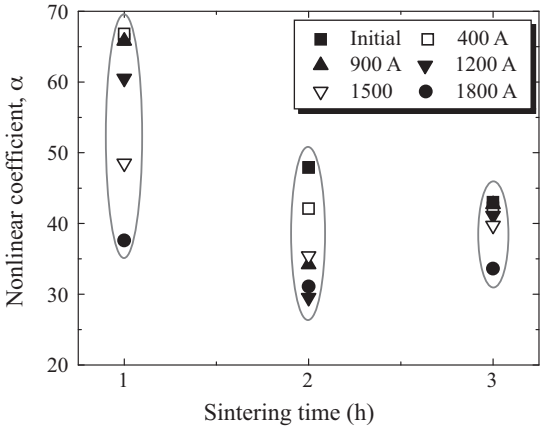

Fig. 6. Variation of nonlinear coefficient of the samples for different sintering times after applying the multi-pulse current.

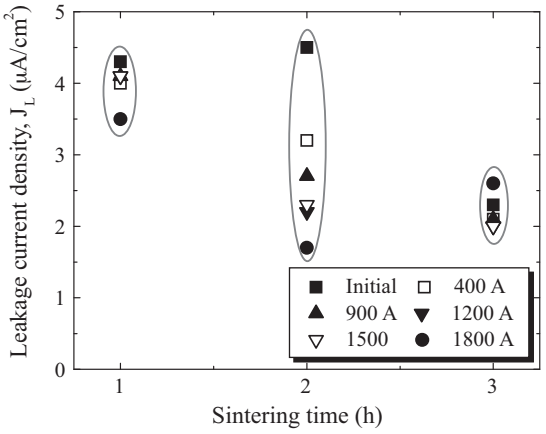

Fig. 7. Variation of leakage current density of the samples for different sintering times after applying the multi-pulse current.

varistors sintered for 3 h could have a direct and positive effect on the field of surge protection devices.

4. Conclusions

The aging behavior against pulse-current of 400–1800 A in the ZnO–Pr_6O_{11}–CoO–Cr_2O_3–Dy_2O_3 varistor ceramics was investigated in accordance with sintering time. The clamp voltage ratio (K) for a pulse-current exhibited a minimum value for the samples sintered for 1 h and a maximum value for the samples sintered for 2 h. The varistor ceramics sintered for 1 h exhibited the best clamp characteristics; the clamp voltage ratio (K) was in the range of $K = 1.69$–1.92 for the lower pulse-current region (5–50 A) and was in the range of $K = 2.0$–2.98 for the higher pulse-current region (400–1800 A). The best electrical stability was obtained by the varistors sintered for 3 h, with $\%\Delta E_{1\,mA/cm^2} = -7.2\%$, $\%\Delta\alpha = -21.9\%$, and $\%\Delta J_L = 13.0\%$ after applying the multi-pulse current of 1800 A.

References

[1] C.-W. Nahm, The electrical properties and d.c. degradation characteristics of Dy_2O_3 doped Pr_6O_{11}-based ZnO varistors, J. Eur. Ceram. Soc. 21 (2001) 545–553.
[2] L.M. Levinson, H.R. Philipp, Zinc oxide varistor – a review, Am. Ceram. Soc. Bull. 65 (1986) 639–646.
[3] T.K. Gupta, Application of zinc oxide varistor, J. Am. Ceram. Soc. 73 (1990) 1817–1840.
[4] Y.S. Lee, T.Y. Tseng, Phase identification and electrical properties in ZnO-glass varistors, J. Am. Ceram. Soc. 75 (1992) 1636.
[5] J. Wong, Microstructure and phase transformation in a highly non-ohmic metal oxide varistor ceramic, J. Appl. Phys. 46 (1975) 1653.
[6] A.B. Alles, V.L. Burdick, The effect of liquid-phase sintering on the properties of Pr_6O_{11}-based ZnO varistors, J. Appl. Phys. 70 (1991) 6883–6890.
[7] A.B. Alles, R. Puskas, G. Callahan, V.L. Burdick, Compositional effect on the liquid-phase sintering of praseodymium oxides-based ZnO varistors, J. Am. Ceram. Soc. 76 (1993) 2098–2102.
[8] Y.-S. Lee, K.-S. Liao, T.-Y. Tseng, Microstructure and crystal phases of praseodymium in zinc oxides varistor ceramics, J. Am. Ceram. Soc. 79 (1996) 2379–2384.
[9] C.-W. Nahm, The nonlinear properties and stability of ZnO–Pr_6O_{11}–CoO–Cr_2O_3–Er_2O_3 ceramic varistors, Mater. Lett. 47 (2001) 182–187.
[10] C.-W. Nahm, J.-S. Ryu, Effect of sintering temperature on electrical properties and stability of Pr_6O_{11}-based ZnO varistors, J. Mater. Sci.: Mater. Electron. 13 (2002) 111–120.
[11] C.-W. Nahm, B. -Shin, S.M.-H. Min, Microstructure and electrical properties of Y_2O_3-doped ZnO–Pr_6O_{11}-based varistor ceramics, Mater. Chem. Phys. 82 (2003) 157–164.
[12] C.-W. Nahm, B.-C. Shin, Effect of sintering time on electrical properties and stability against DC accelerated aging of Y_2O_3-doped ZnO–Pr_6O_{11}-based varistor ceramics, Ceram. Int. 30 (2004) 9–15.
[13] C.-W. Nahm, Microstructure and electrical properties of Dy_2O_3-based ZnO–Pr_6O_{11}-based varistor ceramics, Mater. Lett. 58 (2004) 2252–2255.
[14] C.-W. Nahm, B.-C. Shin, Effect of sintering time on electrical characteristics and DC accelerated aging behaviors of Zn–Pr–Co–Cr–Dy oxide-based varistors, J. Mater. Sci.: Mater. Electron. 16 (2005) 725–732.
[15] C.-W. Nahm, Influence of La_2O_3 additives on microstructure and electrical properties of ZnO–Pr_6O_{11}–CoO–Cr_2O_3-based varistors, Mater. Lett. 59 (2005) 2097–2100.
[16] C.-W. Nahm, Effect of sintering temperature on nonlinear electrical properties and stability against DC accelerated aging stress of (CoO, Cr_2O_3, La_2O_3)-doped ZnO–Pr_6O_{11}-based varistors, Mater. Lett. 60 (2006) 3311–3314.
[17] C.-W. Nahm, Electrical properties and stability of Tb-doped ZnO-based nonlinear resistors, Solid State Commun. 141 (2007) 685–690.
[18] C.-W. Nahm, Effect of cooling rate on electrical properties, impulse surge and dc-accelerated aging behavior of ZPCCD-based varistors, J. Mater. Sci.: Mater. Electron. 20 (2009) 418–424.
[19] C.-W. Nahm, Al doping effect on electrical and dielectric aging behavior against impulse surge in ZPCCYA-based varistors, Mater. Sci. Eng. B 170 (2010) 123–128.
[20] C.-W. Nahm, Electrical behavior against current impulse in ZnO–Pr_6O_{11}-based varistor ceramics with terbium addition, Ceram. Int. 36 (2010) 1495–14501.
[21] C.-W. Nahm, Major effects on impulse aging behavior of ZnO–Pr_6O_{11}–CoO–Cr_2O_3–Er_2O_3 varistor ceramics with small sintering changes, J. Am. Ceram. Soc. 93 (2010) 3056–3059.
[22] C.-W. Nahm, Highly stable nonlinear behavior against impulse current of ZnO–Pr_6O_{11}–CoO–Cr_2O_3–Y_2O_3 varistors, Mater. Lett. 64 (2010) 2631–2634.
[23] C.-W. Nahm, Effect of aluminum doping on electrical and dielectric aging behavior against current impulse of ZPCCY-based varistors, J. Mater. Sci.: Mater. Electron. 22 (2011) 77–83.
[24] J.C. Wurst, J.A. Nelson, Lineal intercept technique for measuring grain size in two-phase polycrystalline ceramics, J. Am. Ceram. Soc. 55 (1972) 109–111.